Supporting Information

Fe$_3$O$_4$ nanoparticles decorated three-dimensional porous carbon/MoS$_2$ composites as anodes for high performance lithium-ion batteries

Youngmoo Jeon[‡a], Jeongyeon Lee[‡a], Myungjin Kim[a], Jiseop Oh[a], Taejin Hwang[a], Yuanzhe Piao*[a, b]

[a] Program in Nano Science and Technology, Graduate School of Convergence Science and Technology, Seoul National University, 145 Gwanggyo-ro, Yeongtong-gu, Suwon–si, Gyeonggi-do, 443-270, Republic of Korea.

[b] Advanced Institutes of Convergence Technology, 145 Gwanggyo-ro, Yeongtong-gu, Suwon–si, Gyeonggi-do, 443-270, Republic of Korea.

‡ These authors contributed equally to this work.

Address correspondence to **parkat9@snu.ac.kr**
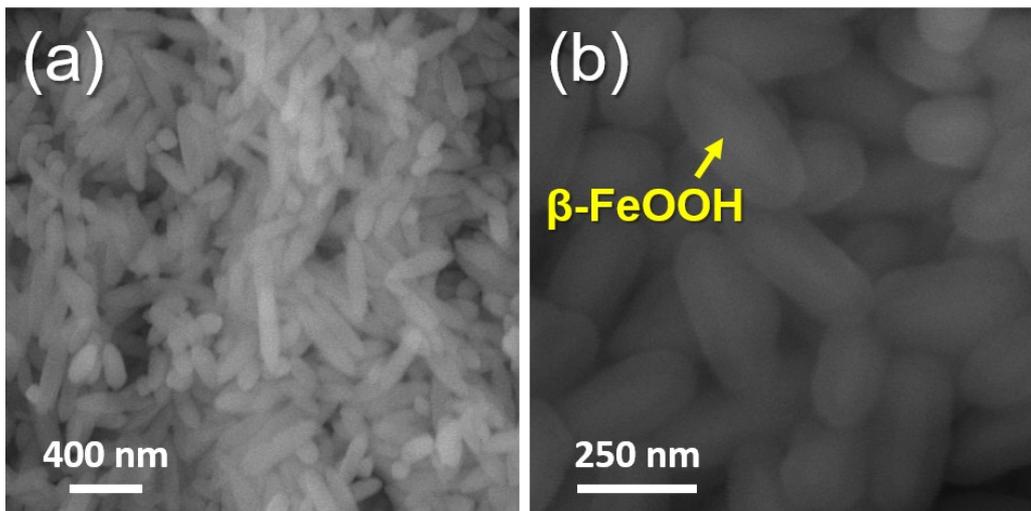
Figure S1   SEM images of (a) β-FeOOH, and (b) SiO$_2$@FeOOH.
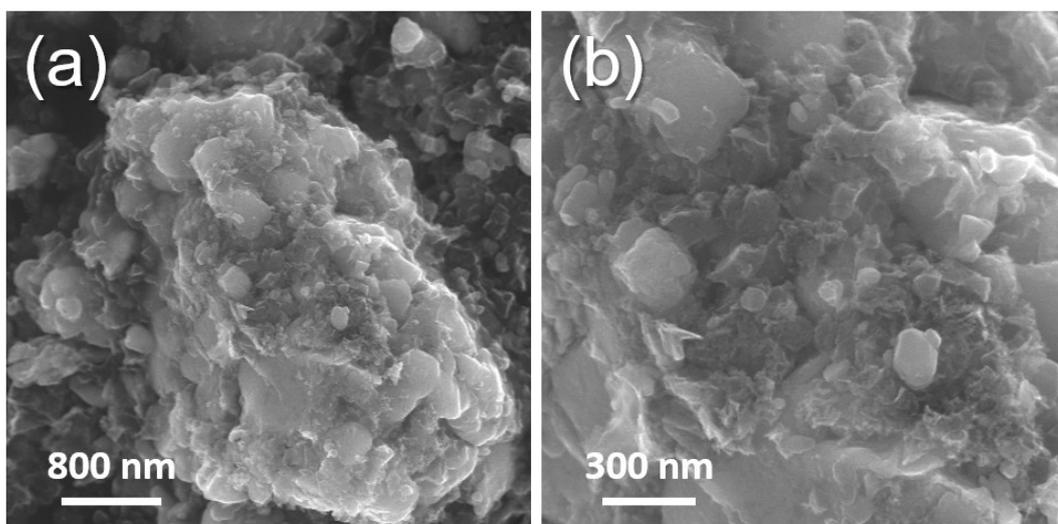
Figure S2 SEM images of BC-MF at (a) low and (b) relatively high magnification.
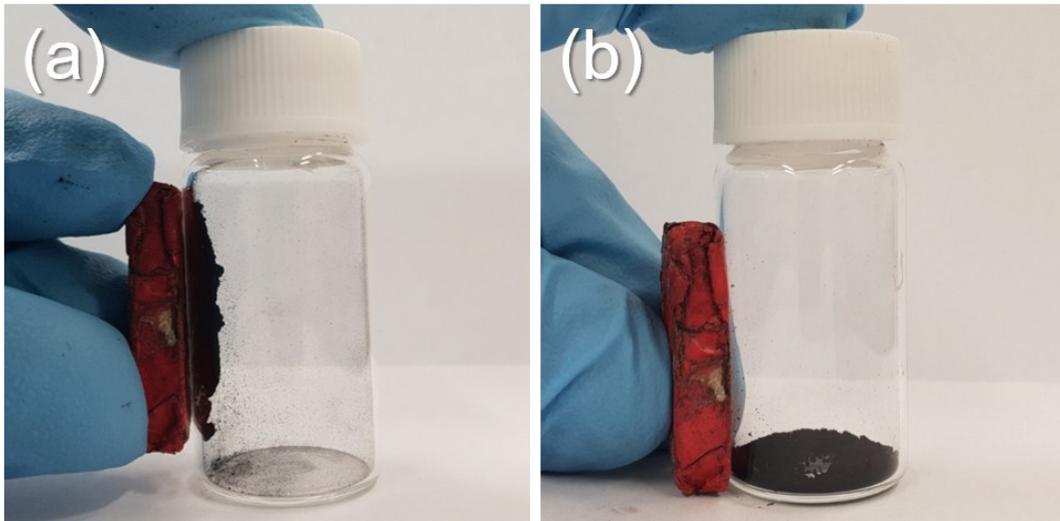
Figure S3   Visual images of (a) C-MF and (b) C-M using an external magnet. The dragging of C-MF to the sidewall of the sample vial confirms the existence of Fe_3O_4 in the sample. While in case of C-M, the etching process leads to the removal of Fe_3O_4.
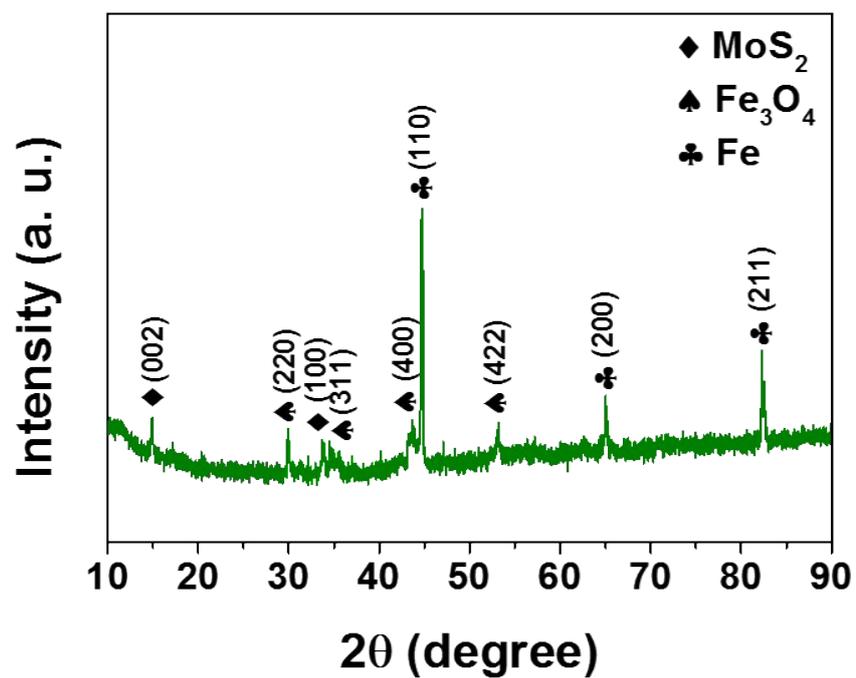
Figure S4 XRD pattern of BC-MF.
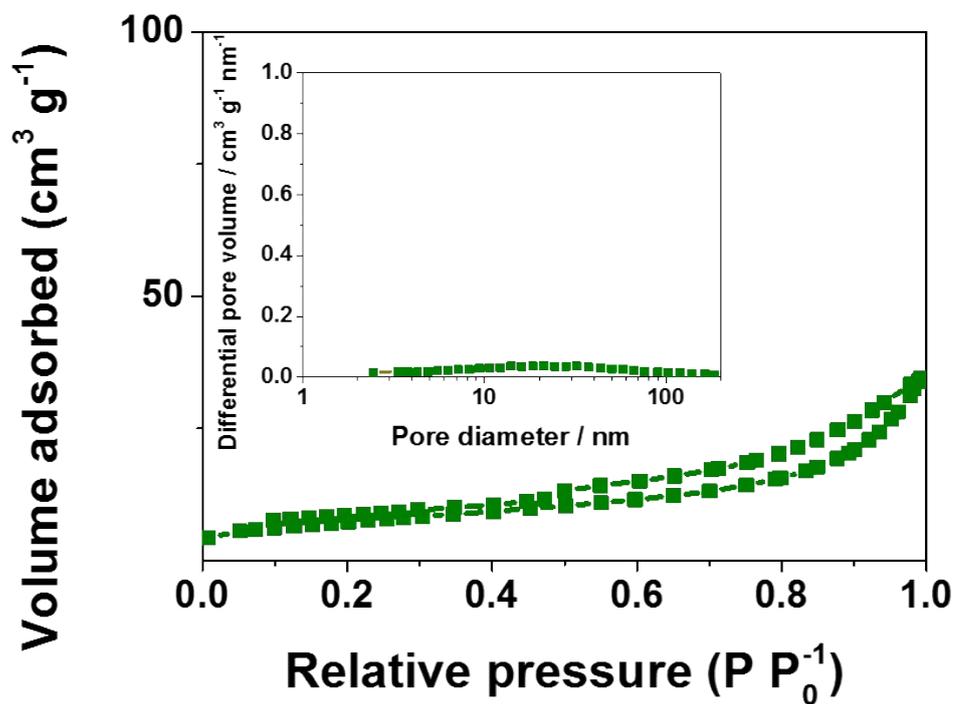
Figure S5 N_2 adsorption-desorption isotherms and pore size distribution (insert) of BC-MF.
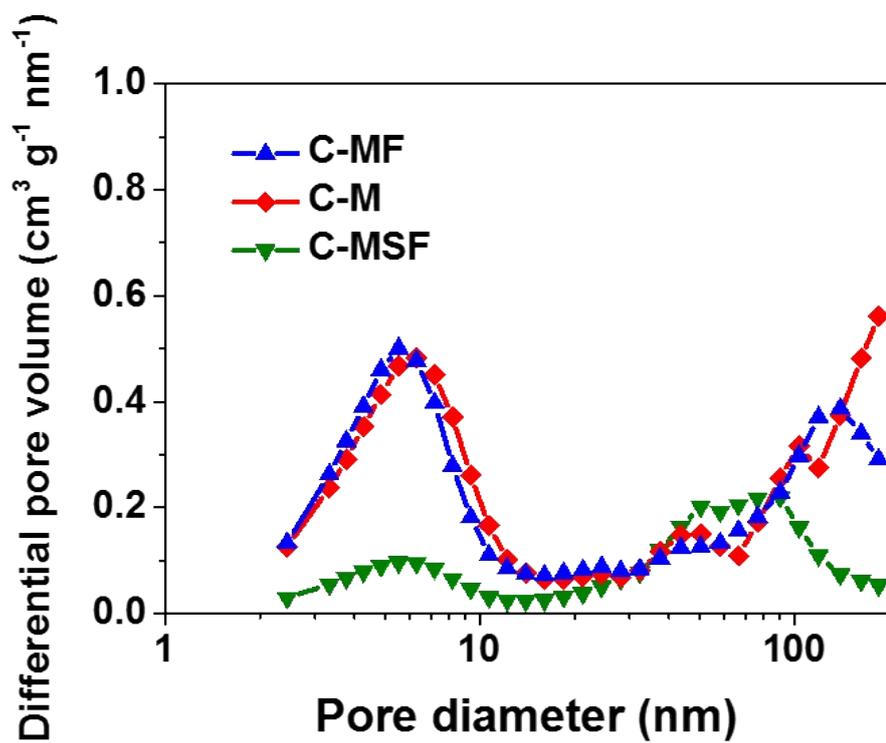
Figure S6   Pore size distributions of C-MF, C-M, and C-MSF.

Table S1   ICP quantitative analysis of samples.

Sample	Mo	Fe
C-MF	2808.3	1143.7
BC-MF	3.71	31.51

The relative concentration of elements (weight ratio)
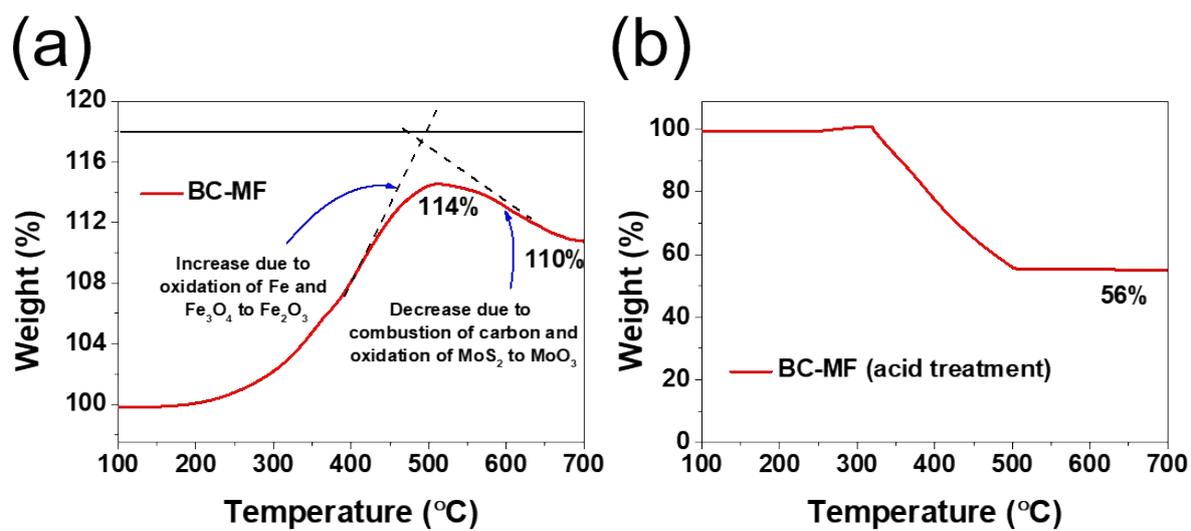
Figure S7 TGA curves of BC-MF (a) before and (b) after acid treatment.
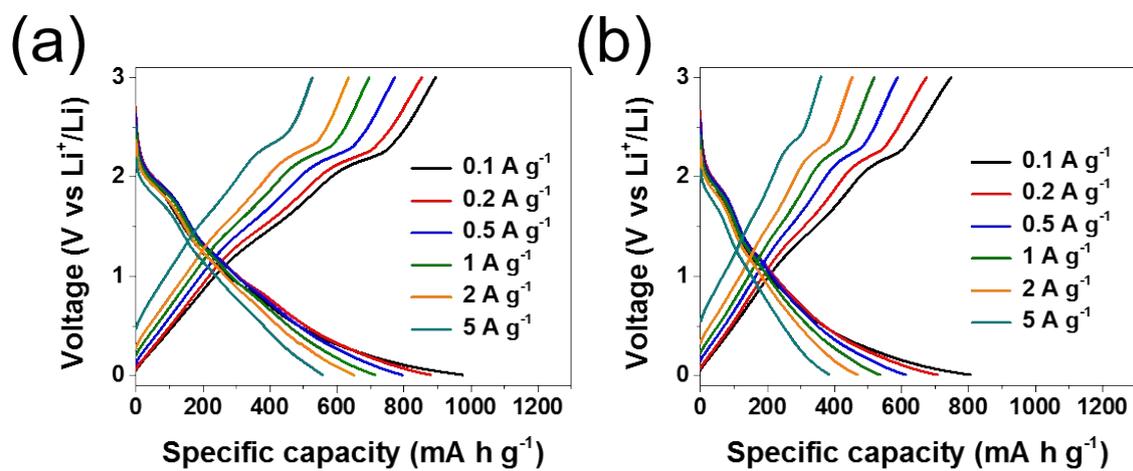
Figure S8　Galvanostatic discharge/charge profiles of (a) C-MF and (b) C-M at different current density.
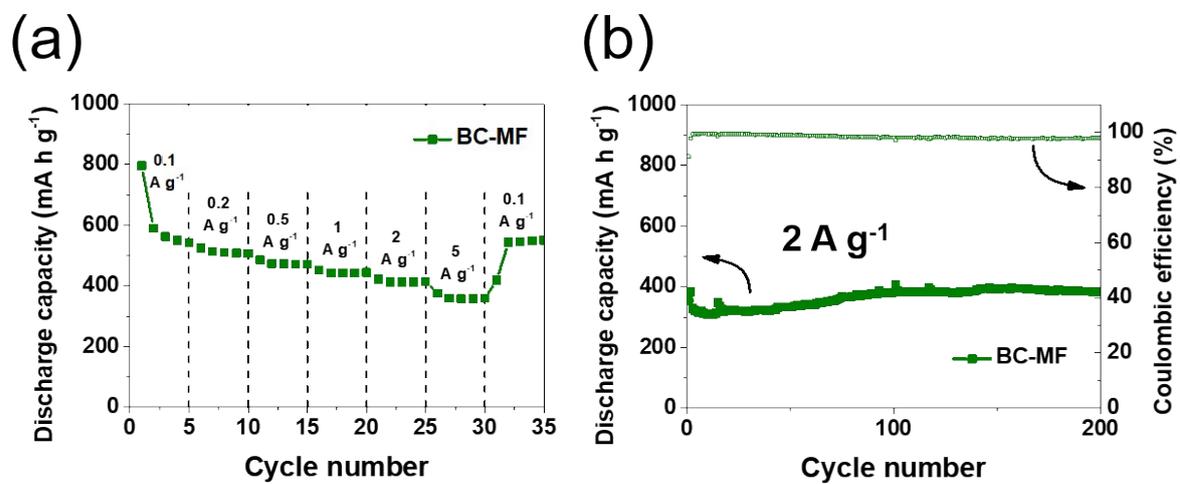
Figure S9   (a) Rate performance of BC-MF at different current densities. (b) Cycling performance of BC-MF at current density of 2 A g^{-1}.
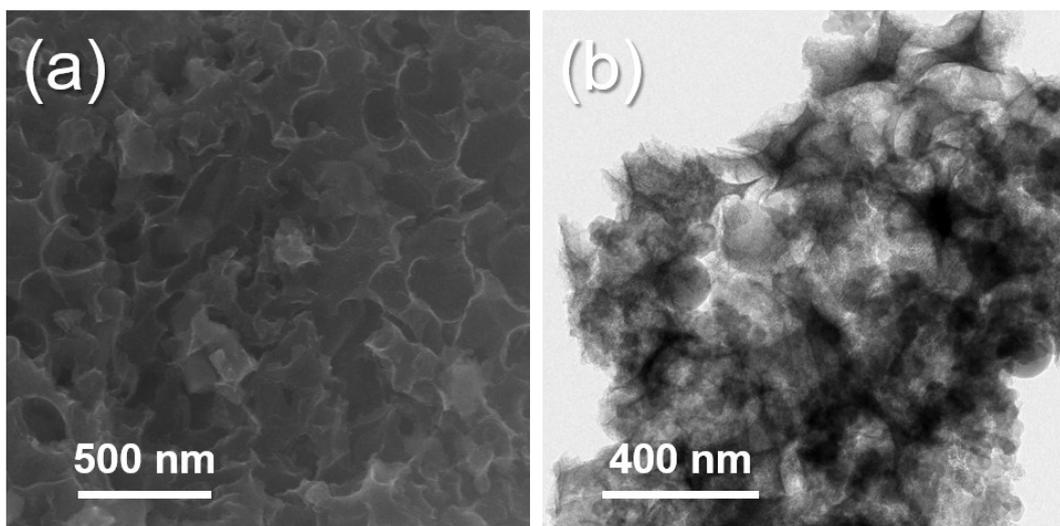
Figure S10   (a) SEM and (b) TEM images of the C-MF electrode after 100 cycles at 2 A g^{-1}.